Numerical analysis of bump solutions for neural field equations with periodic microstructure

Elena Malyutina[a,*], Arcady Ponosov[a], John Wyller[a]

[a]*Department of Mathematical Sciences and Technology, Norwegian University of Life Sciences, P.O. Box 5003, NO-1432 Ås, Norway*

Abstract

We study numerically single bump solutions of a homogenized Amari equation with periodic microvariation. Two attempts are made to detect single bumps that depend on the microvariable. The first attempt which is based on a pinning function technique is applicable in the Heaviside limit of the firing rate function. In the second attempt, we develop a numerical scheme which combines the two-scale convergence theory and an iteration procedure for the corresponding heterogeneous Amari equation. The numerical simulations in both attempts indicate the nonexistence of single bump solutions that depend on the microvariable. Motivated by this result, we finally develop a fixed point iteration scheme for the construction of single bump solutions that are independent of the microvariable when the firing rate function is given by a sigmoidal firing rate function.

Keywords: Rate equations in neuroscience; Periodic; Homogenization

1. Introduction

The Amari equation [1]

$$\frac{\partial}{\partial t}u(x,t) = -u(x,t) + \int_{-\infty}^{\infty} \omega(x-y) f(u(y,t))dy \tag{1}$$

*Corresponding author

Email addresses: elena.malyutina@nmbu.no (Elena Malyutina), arkadi@nmbu.no (Arcady Ponosov), john.wyller@nmbu.no (John Wyller)

is one of the simplest nonlocal field models for the spatiotemporal variation of the neural activity in cortical networks. Here u denotes the average neural activity, ω the coupling strength (referred to as the connectivity function) and f the firing rate function. The actual networks are modelled as a continuous sheet of neurons where the typical spatial and temporal scales of the activity are assumed to be much larger than the corresponding neuronal scales.

The model (1) as well as its modifications and extensions have been used as starting points for the study of traveling waves and localized stationary solutions (so-called *bumps*) and the stability of these coherent structures. A common assumption made in such investigations is that the firing rate function is approximated with the unit step function (Heaviside function). This is convenient from the mathematical point of view as one in that case can find closed form analytical expressions for the traveling waves and the bump solutions. One then carries out the corresponding stability assessment either by a phase space reduction method involving the projection of the dynamics of the full system onto a finite dimensional space in the crossing coordinates between the bumps profiles and the threshold values (i.e. the so-called *Amari approach*) or by means of full stability analysis (i.e. the *Evans function approach*). Moreover, even though no rigorous mathematical justification is given, one tacitly assumes that the Heaviside limit of the firing rate function produces results which represent a sensible approximation to the results obtained in steep but continuous firing rate case. The special case consisting of a one-to-one correspondence between the admissible threshold values and the pulsewidth coordinates, leads to localized stationary solutions called *a single bump solution* (or *a 1-bump solution*) of the model (1). The problem of existence and uniqueness of these solutions has been studied together with their linear stability. See for example Coombes [2] and Bressloff [3] and the references therein.

The problem of deviation from the Heaviside limit of the firing rate function can be resolved in the case when the spectrum of the connectivity kernel is a rational function. In that case the Amari equation (1) can be converted to an ODE which possesses a Hamiltonian structure. The existence of bumps is then resolved by means of standard techniques for such systems i.e. detecting the homoclinic orbits of the system. See for example [4] and [5]. In the general case with no specific assumptions imposed on the connectivity kernel,

existence of stationary solutions is proved using functional analytical techniques (fixed point theorems) as well as their dependence on the steepness parameter of the firing rate function is explored [6, 7, 8, 9]. For the purpose of constructing the actual stationary solutions one has to rely on different numerical schemes. Coombes *et al.* [10] has proposed an iteration scheme for construction of single bump solutions of the Amari equation (1) in the case of a sigmoidal firing rate function, without actually given any rigorous justification of the approach. In Oleynik *et al.* [11] two iteration schemes for constructing single bump solutions in the case of sigmoidal firing rate function are proposed. A rigorous justification of the convergence properties of these schemes is also given. The first scheme is a bumps width iteration method which generalizes the method proposed in Coombes *et al.* [10] while the second one is a fixed point iteration procedure based on Kishimoto *et al.* [6]. In [7] the spatial domain is assumed to be bounded and the firing rate functions sigmoidal. Here the fixed point structure of the stationary problem is exploited in the numerical construction procedure for the bumps solutions.

The modelling framework (1) and many of its extensions presuppose that the medium is homogeneous and isotropic. Hence one does not not take into account the microscopic fine structure which obviously is present in the cortex. Modelling of these effects is therefore important and has hence been subject to much research effort in the the neuroscience community. See for example Bressloff [3] and the references therein. One way of tackling the coupling of macro- and microstructure problem in neural field models is by using *homogenization techniques* [12, 13]. When the medium possesses a periodic microstructure, the homogenization results in an averaging over some well identified microscale. In the neural field theory context the coupling between periodic micro level structure of the cortex and nonlocal mean field description has been investigated in the works [14, 15, 16, 18, 17, 19]. It turns out that the detailed microstructure has an impact on pattern forming mechanisms as well as existence and stability of traveling fronts and pulses.

Standard homogenization techniques consist of different type of perturbation expansions (see for example Persson *et al.* [20] and the references therein). Modern homogenization theory based on multi-scale convergence theory represents an alternative and rigorous approach to this problem. It yields efficient and rigorous methods for studying the coupling between the microstructure and macroscopic levels. The multiscale technique was orig-

inally presented by Nguetseng [21]. A review of the method is given in Lukkassen *et al.* [22].

In [23], [24] and [25] it is shown that the nonlocal neural field model

$$\frac{\partial}{\partial t}u_\varepsilon(x,t) = -u_\varepsilon(x,t) + \int_\Omega \omega(x'-x, \frac{x'-x}{\varepsilon})f(u_\varepsilon(x',t))dx' \qquad (2)$$

converges to

$$\frac{\partial}{\partial t}u(x,y,t) = -u(x,y,t) + \int_\Omega dx' \int_Y dy'\omega(x'-x,y'-y)f(u(x',y',t)) \qquad (3)$$

in the two-scale sense when $\varepsilon \to 0$. Here $x \in \Omega \subseteq \mathbb{R}^N$, $t > 0$. The connectivity kernel ω by assumption is periodic in the second argument $y = \frac{x}{\varepsilon}$, i.e. $\omega_\varepsilon(x) = \omega(x, \frac{x}{\varepsilon})$. A key feature in the derivation of (3) from (2) is the exploitation of Visintin's theorem on two-scale convergence of convolution integrals [26]. This result enables us to get the correct limit of the convolution term in (2) as $\varepsilon \to 0$. Svanstedt *et al.* [24] construct the y-independent single bump solutions of the homogenized equation (3) by using the pinning function technique in the case of Heaviside step firing function. In the same paper stability theory for these bumps is developed. Just as in the translational invariant case (1) intervals for which the pinning function is increasing correspond to unstable bumps, while for the complementary regimes with a decreasing pinning function the corresponding bumps are stable.

This serves as a background for the present paper.

In this paper we first of all give numerical evidence for the nonexistence of y-dependent single bump solutions. We demonstrate this in two different ways: First of all, we use a pinning function technique which generalizes the method developed in Svanstedt *et al.* [24]. This method is applicable to the case when the firing rate function is given by means of the Heaviside step function. Secondly, we make use of a combination of the iteration method for single bumps developed in Oleynik *et al.* [11] and the two-scale convergence superposition method described in Visintin [26]. The latter method is designed for constructing single bump solutions of the homogenized Amari

equation (3) in the case of the sigmoidal firing rate function. Then, as consequence of these two attempts to construct single bumps of (3) with a nontrivial variation in the local variable y, we embark on formulating a numerical scheme for iterative construction of y-independent single bumps of (3).

We organize the present paper as follows: In Section 2 we present the stationary versions of the models (2) and (3) and the assumptions imposed on the connectivity kernel and the firing rate function. Section 3 is devoted to the two attempts to construct for y-dependent single bump solutions numerically. In Section 4 we construct y-independent single bump solutions of (3) by means of a direct iteration scheme. Section 5 contains the conclusions and outlook.

2. The stationary heterogeneous and homogenous Amari models

The stationary versions of the heterogeneous and homogenized Amari models are given as the fixed point problems

$$U_\varepsilon(x) = \int_{-\infty}^{\infty} \omega_\varepsilon(x - x') f(U_\varepsilon(x'))dx' \tag{4}$$

and

$$U(x, y) = \int_0^1 \int_{-\infty}^{\infty} \omega(x - x', y - y') f(U(x', y'))dx'dy' \tag{5}$$

respectively. The y-independent stationary solutions of the homogenized Amari model (5) must satisfy the fixed point problem

$$U(x) = \int_{-\infty}^{\infty} \langle\omega\rangle(x - x') f(U(x'))dx' \tag{6}$$

where $\langle\omega\rangle$ is the mean value of the connectivity kernel ω, i.e.

$$\langle\omega\rangle(x) = \int_0^1 \omega(x, y)dy \tag{7}$$

In the present work the connectivity kernel ω is assumed to be expressed in terms of the scaling function φ and the synaptic footprint function σ, i.e.

$$\omega(x,y) = \frac{1}{\sigma(y)}\varphi[\frac{x}{\sigma(y)}] \tag{8}$$

where σ is given as

$$\sigma(y) = 1 + \gamma\cos(2\pi y), \quad \gamma \in [0,1) \tag{9}$$

The scaling function $\varphi : \mathbb{R} \to \mathbb{R}$ is assumed to be spatially symmetric ($\varphi[\xi] = \varphi[-\xi]$), absolute integrable ($\int_{-\infty}^{\infty} |\varphi[\xi]|d\xi < \infty$), continuous, bounded and piecewise smooth. In this work the scaling function φ will be given as the wizard hat function

$$\varphi(\xi) = e^{-|\xi|}(1 - \alpha|\xi|), \quad \alpha > 0 \tag{10}$$

and the difference of Gaussian functions

$$\varphi(\xi) = Ke^{-kx^2} - Me^{-mx^2}, \quad K > M > 0, \ k > m > 0 \tag{11}$$

Due to the properties of the scaling function φ and synaptic footprint function σ, the connectivity kernel ω satisfies the the same set of properties as the scaling function φ: It is spatially symmetric w.r.t. first variable ($\omega(-x,y) = \omega(x,y)$), absolute integrable on $\mathbb{R}$ for each $y \in [0,1]$, continuous, bounded and piecewise smooth in (x,y).

The firing rate function f is assumed to be smooth, i.e. it satisfies the following general properties

- $f : \mathbb{R} \to [0,1]$,
- f' is continuous and bounded,
- $f'(u) \geqslant 0$,
- $\lim_{u\to-\infty} f(u) = 0$, $\lim_{u\to+\infty} f(u) = 1$.

In the present paper we consider firing rate functions where derivative has compact support, i.e. $f(u) = 0$ if $u \leqslant 0$ and $f(u) = 1$ if $u \geqslant \tau$ with $\tau > 0$:

$$f(u) = \begin{cases} 0, & u \leqslant 0 \\ \phi(u), & 0 < u < \tau \\ 1, & u \geqslant \tau \end{cases}, \tag{12}$$

where $\tau > 0$, ϕ is an arbitrary smooth, monotonically increasing, and normalized function with the additional property

$$\phi(0) = 0, \quad \phi(\tau) = 1.$$

We refer to the parameter τ as the *smoothness parameter* and the firing rate function (12) as the *sigmoidal firing rate function*.

As an example of a firing rate function of the type (12) we have

$$f(u) = \begin{cases} 0, & u \leqslant \theta \\ \dfrac{(u-\theta)^p}{(u-\theta)^p + (1-(u-\theta))^p}, & \theta < u < \theta + \tau, \\ 1, & u \geqslant \theta + \tau \end{cases}, \tag{13}$$

where the parameter p is positive. Here θ plays the role as the threshold value for firing of the neural activity.

When $\tau \to 0$, the firing rate function (12) approaches the Heaviside step function H i.e.

$$f(u) = H(u-\theta) = \begin{cases} 0, & u < \theta \\ 1, & u \geqslant \theta \end{cases}, \tag{14}$$

In Oleynik *et al.* [11] two iteration methods for constructing spatially symmetric single bump solution $U(x)$ of the integral equation

$$U(x) = \int_{-\infty}^{\infty} \omega(x - x') f(U(x'))dx' \tag{15}$$

were developed in the case of sigmoidal firing rate function (13). In that paper the squeezing property observed in Kishimoto *et al.* [6] for stationary solutions

$$U_\tau(x) \leq U(x) \leq U_0(x) \tag{16}$$

was exploited in one of the iteration schemes referred to as the direct iteration scheme. Here U_0 and U_τ are solutions of (15) corresponding to the firing rate functions f_0 and f_τ given as

$$f_0(u) = H(u-\theta), \quad f_\tau(u) = H(u-(\theta+\tau)) \tag{17}$$

Kishimoto *et al.* [6] and Oleynik *et al.* [11] refer to the model (15) with the firing rate functions f_0, f_τ, and f as the f_0-, $f_\tau-$, and $f-$ field model, respectively.

A notable feature which is analogous to the squeezing property (16) is that the solutions $U_\varepsilon(x)$, $U(x,y)$ and $U(x)$ of (4), (5) and (6), respectively, with the firing rate function given by (12) satisfies the squeezing property of the Kishimoto–Amari type

$$U^\tau_\varepsilon(x) \le U_\varepsilon(x) \le U^0_\varepsilon(x) \tag{18}$$

$$U^\tau(x,y) \le U(x,y) \le U^0(x,y) \tag{19}$$

$$U^\tau(x) \le U(x) \le U^0(x) \tag{20}$$

Here U^μ_ε, $U^\mu(x,y)$ and $U^\mu(x)$ (with $\mu = 0, \tau$) are stationary solutions of (4), (5) and (6), respectively, with firing rate function given by (17). Just as in Kishimoto *et al.* [6] and Oleynik *et al.* [11] we refer to the models (4), (5) and (6) with the firing rate functions f_0, f_τ, and f as the f_0-, $f_\tau-$, and $f-$ field models, respectively.

In Svanstedt *et al.* [24] the existence and stability of single bump solutions of the homogenized Amari equation (6) were studied in the f_0- case by means of pinning function technique. Just as in Oleynik *et al.* [11] and in accordance with the bounds (19) and (20) we can squeeze a single bump solution in the sigmoidal case in between the known single bumps solutions U_τ and U_0. We will exploit this fact in the subsequent sections. In the present paper we will give numerical evidence for the conjecture that any bump solution of the homogenized Amari equation is independent of the local variable y i.e. it satisfies (6).

3. Nonexistence of y-dependent solutions of the homogenized Amari equation

In this section we demonstrate in detail the two attempts to construct y-dependent solutions of (5). The first attempt is based on a generalization

of the pinning functions technique developed in Svanstedt *et al.* [24]. This method is applicable to the case when the firing rate function is given by means of the Heaviside step function (14). The second attempt is based on a combination of the iteration method for single bumps developed in Oleynik *et al.* [11] and the two-scale convergence superposition method described in Visintin [26]. This method is designed for constructing the single bump solutions of the homogenized Amari equation (6) in the case of the sigmoidal firing rate function (13). Numerical experiments based in these two attempts indicate that the single bump solutions are y-independent.

3.1. Bumps width method

Let us consider solutions of stationary problem (5) when the firing rate function f is modeled by means of the Heaviside step function (14). The solution $U(x, y)$ is assumed to be symmetric with respect to first variable x, i.e. $U(-x, y) = U(x, y)$ for all $x \in \mathbb{R}, y \in \mathbb{R}$ and 1-periodic in the variable y, i.e. $U(x, y) = U(x, y + 1)$ for all $x \in \mathbb{R}, y \in \mathbb{R}$. Due to the 1-periodicity of $U(x, y)$ in the y-variable it is only necessary to study the bumps construction problem for $y \in [0, 1)$.

For the sake of completeness we first recall the construction of single bumps as outlined in Svanstedt *et al.* [24]. One starts out by assuming that there exists a unique $\Delta > 0$ such that the stationary solution $U(x)$ satisfies $U(\Delta) = \theta$. Δ is referred to as the bumps width. Therefore, the stationary solution can be written in terms of the pinning function W as

$$U(x) = W(\Delta - x) + W(\Delta + x) \tag{21}$$

where the pinning function is the antiderivative

$$W(L) = \int_0^L \langle\omega\rangle(x)dx \tag{22}$$

of the mean value $\langle\omega\rangle$ defined by (7). The bump width Δ can now be found from the pinning condition

$$W(2\Delta) = \theta \tag{23}$$

Our aim is to generalize the pinning function technique of Svanstedt *et al.* [24] by allowing the bump width Δ to be y-dependent: $\Delta = \Delta(y)$. The

crossing condition between the bumps and the threshold value θ now reads

$$U(\Delta(y), y) = \theta, \quad y \in [0, 1) \tag{24}$$

Since the firing rate function f is assumed to be modeled by means of Heaviside step function (14), we formally obtain the expression

$$U(x, y) = \int_0^1 \int_{-\Delta(y)}^{\Delta(y)} \omega(x - x', y - y') dx' dy' \tag{25}$$

for the single bump solution. The next step consists of deriving the counterpart of the pinning condition (24). We proceed as follows: Introduce the anti - derivative Φ of the scaling function φ

$$\Phi[\eta] = \int_0^{\eta} \varphi[\xi] d\xi \tag{26}$$

The expression (25) can be rewritten as

$$U(x, y) = \int_0^1 F(\sigma(y - y'), x, \Delta(y')) dy' \tag{27}$$

where the integrand F is defined as

$$F(\sigma(z), x, \Delta(y')) \equiv \Phi\Big[\frac{\Delta(y') + x}{\sigma(z)}\Big] + \Phi\Big[\frac{\Delta(y') - x}{\sigma(z)}\Big]$$

The pinning condition (24) now reads

$$\int_0^1 F(\sigma(y - y'), \Delta(y), \Delta(y')) dy' = \theta \tag{28}$$

The nonlinear Fredholm equation (28) serves as the starting point for determining the bumps width. Due to the dependency of function F on $z = y - y'$, $\Delta(y)$ and $\Delta(y')$ in (28) standard numerical methods for solving nonlinear equations (such as Euler's method) are not applicable. Instead we proceed

as follows: We divide the unit interval $[0,1]$ into n equidistant subintervals $[y_0, y_1], [y_1, y_2], \ldots, [y_{n-1}, y_n]$ where the partitioning points $y_0, y_1, \ldots, y_{n-1}, y_n$ are given as $y_0 = 0$, $y_1 = y_0 + h$,..., $y_{n-1} = y_0 + (n-1)h$, $y_n = 1$, with the stepping length $h = 1/n$. The integral on the left hand side of (28) is now approximated my means of an ordinary Riemann's sum i.e.

$$\int_0^1 F(\sigma(y - y'), \Delta(y), \Delta(y'))dy' \simeq \sum_{i=0}^{n-1} F(\sigma(y - y_i), \Delta(y), \Delta(y_i))h$$

Then for each $y = y_j$, $(j = 0, 1, \ldots, n-1)$ we get the following system of n nonlinear equations

$$\sum_{i=0}^{n-1} F(\sigma(y_j - y_i), \Delta(y_j), \Delta(y_i)) \cdot h = \theta, \quad \text{for } j = 0, 1, \ldots, n-1. \tag{29}$$

for the determination of the sequence of bumps width values $\Delta_0 \equiv \Delta(y_0)$, $\Delta_1 \equiv \Delta(y_1)$, ..., $\Delta_{n-1} \equiv \Delta(y_{n-1})$.

In order to solve the system (29) numerically by means of MATLAB, we define the initial guess which is required by the MATLAB Optimization Toolbox for solving the system of nonlinear equations. The method for solving the system of nonlinear equations is based on the trust region fsolve algorithm. See Mor *et al.* [27] and the references therein for details. In our simulations we have used very many different initial guesses $\Delta^{(0)}(y)$ of the solution $\Delta(y)$ such as

$$\Delta^{(0)}(y) = A\cos(a(y + c)) + C, \tag{30}$$

$$\Delta^{(0)}(y) = B\sin(b(y + d)) + D, \tag{31}$$

where A, a, B, b, C, c, D, d are arbitrary constants which do make $\Delta^{(0)}(y)$ 1-periodic. In all the computations we fixate the number of intervals and the stepping length in the discretization (29) to be $n = 80$ and $h = 0.0125$, respectively. We also assume that $\theta = 0.15$. Figs. 1 and 2 show the outcome of the numerical simulations in the case of the scaling functions (10) and (11), respectively. It turns out that the numerically obtained bumps width $\Delta(y)$ remain constant in all the cases we have investigated within the error margins in the numerical computation. We have chosen to approximate this constant with Δ_{mean} of the sequence $\Delta_0 \equiv \Delta(y_0)$, $\Delta_1 \equiv \Delta(y_1)$, ..., $\Delta_{n-1} \equiv \Delta(y_{n-1})$

i.e.

$$\Delta(y) \approx \Delta_{mean} = \frac{1}{n} \sum_{i=0}^{n} \Delta_i \tag{32}$$

which is graphically depicted in Figs. 1 and 2. The same figures display the numerical error ε_{abs} obtained in the computation i.e.

$$\begin{gathered} \varepsilon_{abs} = \Delta_{\max} - \Delta_{\min}, \\ \Delta_{\max} = \max_{0 \leqslant i \leqslant n} \Delta_i, \; \Delta_{\min} = \min_{0 \leqslant i \leqslant n} \Delta_i \end{gathered} \tag{33}$$

The tables 1 and 2 summarize the error estimates obtained in the numerical simulations, thus supporting the conjecture that the bumps width Δ is independent of y in case of scaling functions (10) and (11), respectively. Here the relative error ε_{rel} is defined as

$$\varepsilon_{rel} = \frac{\varepsilon_{abs}}{\Delta_{mean}} \tag{34}$$

Fig. 3 shows the variation of the bumps width Δ_{mean} with the heterogeneity parameter γ in case of scaling functions (10) and (11) for $\theta = 0.15$. In Fig. 4 we compare the results for dependency of bumps width of the solutions of y-dependent and y-independent fixed point problems (5) and (6), respectively, on the heterogeneity parameter γ. Basically, we compare the Fig. 3a with the result from Svanstedt *et.al.*[24], and see that the shapes of the curves are the same, while the values of the parameter γ which correspond to the switching from existence to nonexistence (green stars) are different. This difference may be due to numerical errors since the value Δ is plotted more precise than Δ_{mean} which is calculated as a mean value of the roots of the system of n nonlinear equations. We do not pursue this issue, however, as our aim was to support the conjecture that the bumps are y-independent.

3.2. The superposition method

In this section we look for y-dependent stationary solutions of the heterogeneous Amari equation (2) in case of the sigmoidal firing rate function (13), i.e. we consider the solutions of the fixed point problem (4). We proceed by using combination of the methods developed in Oleynik *et al.* [11] and Visintin [26].

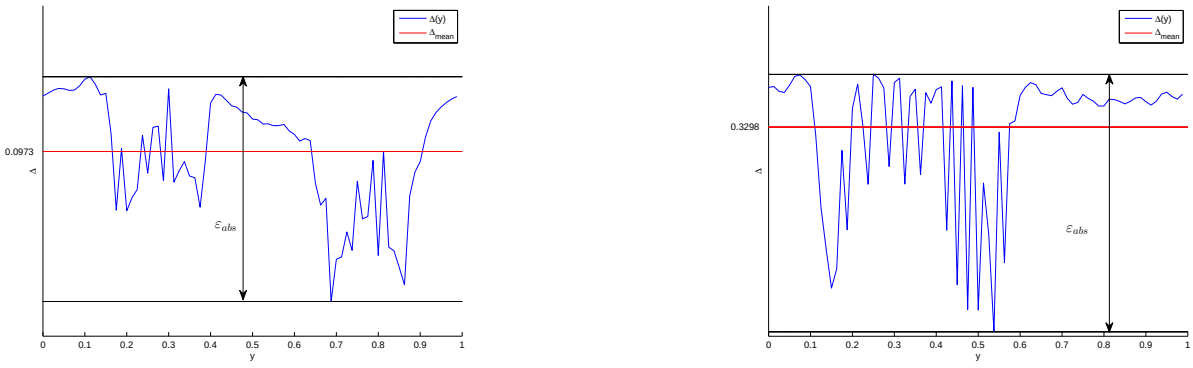

(a) (b)

Figure 1: The bumps width as a function of the local variable y for narrow (Fig. 1a) and broad (Fig. 1b) bumps in the case of the scaling function (10). The number of intervals and the stepping length in the discretization (29): $n = 80$, $h = 0.0125$. Other input data: $\gamma = 0.5$, $\theta = 0.15$, $\alpha = 2$. The absolute and relative errors are $\varepsilon_{abs} = 2.72 \cdot 10^{-8}$, $\varepsilon_{rel} = 2.79 \cdot 10^{-7}$ ($B = -0.7$, $b = 4\pi$, $d = 0.1$, $D = 1.1$) and $\varepsilon_{abs} = 3.12 \cdot 10^{-9}$, $\varepsilon_{rel} = 9.46 \cdot 10^{-9}$ ($B = -0.3$, $b = 4\pi$, $d = 0.4$, $D = 0.8$) for narrow and broad bumps, respectively.

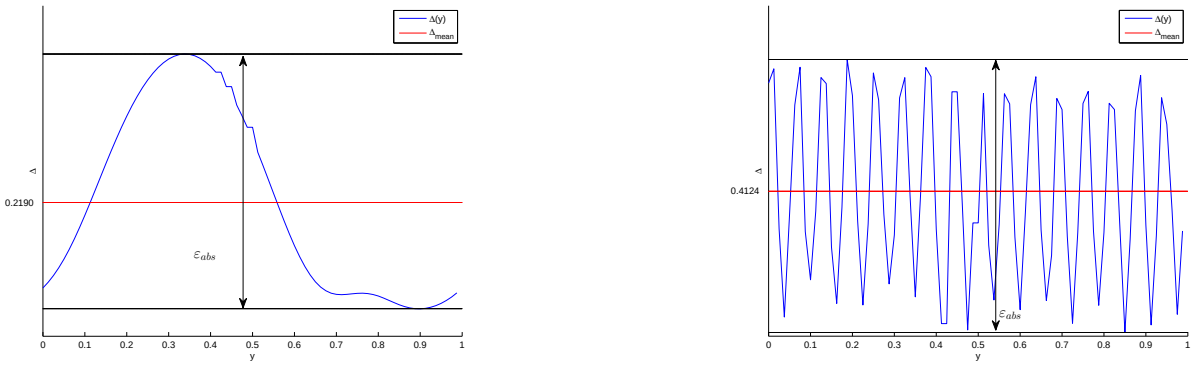

(a) (b)

Figure 2: The bumps width as a function of the local variable y for narrow (Fig. 2a) and broad (Fig. 2b) bumps in the case of the scaling function (11). The number of intervals and the stepping length in the discretization (29): $n = 80$, $h = 0.0125$. Other input data: $\gamma = 0.5$, $\theta = 0.15$, $K = 1.5$, $k = 2$, $M = 1$, $m = 1$. The absolute and relative errors are $\varepsilon_{abs} = 3.86 \cdot 10^{-4}$, $\varepsilon_{rel} = 1.76 \cdot 10^{-3}$ ($B = 0.2$, $b = 2\pi$, $d = 0.4$, $D = 0.1$) and $\varepsilon_{abs} = 1.91 \cdot 10^{-9}$, $\varepsilon_{rel} = 4.63 \cdot 10^{-9}$ ($B = 0.2$, $b = 4\pi$, $d = 0.2$, $D = 0.6$) for narrow and broad bumps, respectively.

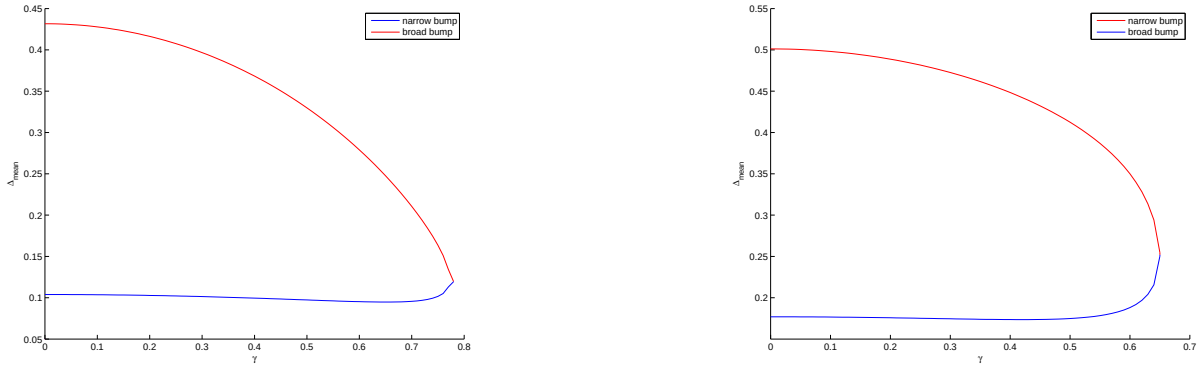

(a) (b)

Figure 3: The bumps width Δ_{mean} as a function of the heterogeneity parameter γ in the case of the scaling function (10) with $\alpha = 2$ (Fig. 3a) and the scaling function (11) with $K = 1.5$, $k = 2$, $M = 1$, $m = 1$ (Fig 3b). The number of intervals and the stepping length in the discretization (29): $n = 80$, $h = 0.0125$. The threshold value: $\theta = 0.15$.

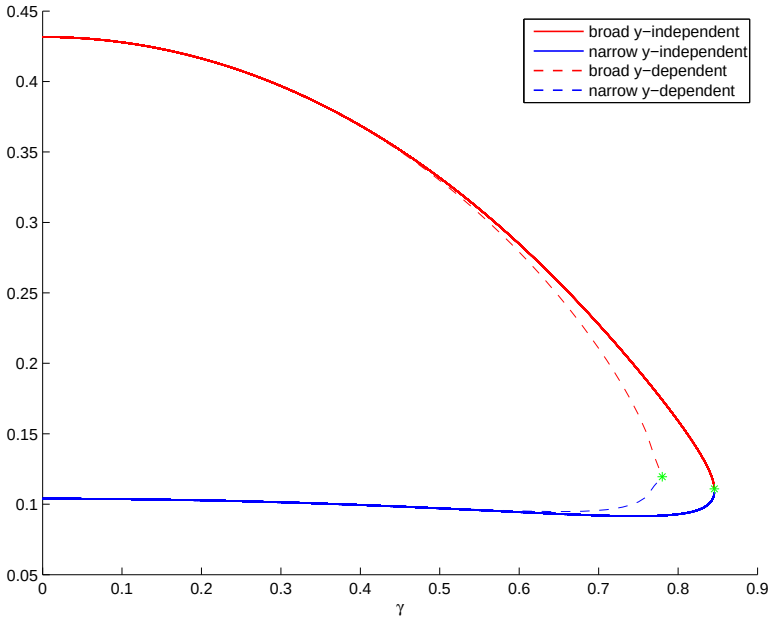

Figure 4: The width Δ_{mean} of 1-bump solution of y-dependent fixed point problem (5) as a function of the heterogeneity parameter γ – dashed line, and the width Δ of 1-bump solution of y-independent fixed point problem (6) as a function of the heterogeneity parameter γ – bold line in the case of the scaling function (10). The green stars are the merging points of narrow (blue) and broad (red) bumps widths. Input data: $\alpha = 2$, $n = 80$, $h = 0.0125$, $\theta = 0.15$.

Table 1: The absolute and relative errors in the computation of the narrow and broad bumps widths in case of the scaling function (10). Input data: $n = 80$, $h = 0.0125$, $\theta = 0.15$, $\alpha = 2$.

Narrow bumps widths errors

B	b	d	D	ε_{abs}	ε_{rel}	Δ_{mean}
-0.7	4π	0.1	1.1	$2.72 \cdot 10^{-8}$	$2.79 \cdot 10^{-7}$	0.0973
0.5	4π	0.3	1	$1.44 \cdot 10^{-10}$	$1.48 \cdot 10^{-9}$	0.0973
-0.8	4π	-0.1	0.9	$2.73 \cdot 10^{-9}$	$2.81 \cdot 10^{-8}$	0.0973
0.8	2π	0.2	1.2	$1.35 \cdot 10^{-7}$	$1.39 \cdot 10^{-6}$	0.0973
0.9	2π	0.4	1.3	$2.40 \cdot 10^{-9}$	$2.46 \cdot 10^{-8}$	0.0973

Broad bumps widths errors

B	b	d	D	ε_{abs}	ε_{rel}	Δ_{mean}
-0.3	2π	0.4	0.8	$3.12 \cdot 10^{-9}$	$9.46 \cdot 10^{-9}$	0.3298
0.4	2π	0.2	0.5	$1.22 \cdot 10^{-8}$	$3.70 \cdot 10^{-8}$	0.3298
-0.5	4π	0.5	0.9	$8.15 \cdot 10^{-9}$	$2.47 \cdot 10^{-8}$	0.3298
0.6	4π	0.6	0.7	$1.00 \cdot 10^{-8}$	$3.04 \cdot 10^{-8}$	0.3298
-0.6	4π	0.7	1.3	$5.08 \cdot 10^{-8}$	$1.54 \cdot 10^{-7}$	0.3298

It is easy to check that the connectivity kernel ω_ε satisfies the same properties as the connectivity kernel ω due to the properties of scaling function φ and synaptic footprint function σ. This enables us to propose an iteration method for constructing single bump solutions of (4) in a way analogous to Oleynik *et al.* [11] for single bumps in (15).

We assume that the bump solution U_ε is spatially symmetric and localized: $U_\varepsilon(-x) = U_\varepsilon(x)$ and $U_\varepsilon(\pm\infty) = 0$. Moreover, we assume that there exist $\Delta > 0$ and small $\delta > 0$ such that

$$\begin{aligned} &U_\varepsilon(x) > \theta, \quad |x| < \Delta - \delta; \\ &U_\varepsilon(x) < \theta, \quad |x| > \Delta + \delta \end{aligned} \tag{35}$$

which means that the crossing condition $U_\varepsilon(x) = \theta$ has at least one positive solution. The equation (4) can now be expressed as

$$U_\varepsilon(x) = \int_0^\infty r_\varepsilon(x, x') f(U_\varepsilon(x'))dx', \quad \varepsilon > 0$$

Table 2: The absolute and relative errors in the computation of the narrow and broad bumps widths in case of the scaling function (11). Input data: $n = 80$, $h = 0.0125$, $\theta = 0.15$, $K = 1.5$, $k = 2$, $M = 1$, $m = 1$.

Broad bumps widths errors

B	b	d	D	ε_{abs}	ε_{rel}	Δ_{mean}
0.3	2π	0.3	0.7	$1.89 \cdot 10^{-9}$	$4.58 \cdot 10^{-9}$	0.4124
0.1	2π	0.1	0.7	$2.78 \cdot 10^{-9}$	$6.74 \cdot 10^{-9}$	0.4124
0.2	4π	0.2	0.6	$1.91 \cdot 10^{-9}$	$4.63 \cdot 10^{-8}$	0.4124
0.4	4π	0.3	0.6	$1.89 \cdot 10^{-9}$	$4.59 \cdot 10^{-9}$	0.4124
0.2	2π	0.7	0.5	$1.89 \cdot 10^{-9}$	$4.59 \cdot 10^{-9}$	0.4124

Narrow bumps widths errors

B	b	d	D	ε_{abs}	ε_{rel}	Δ_{mean}
0.5	2π	0.6	0.4	$9.17 \cdot 10^{-4}$	$3.07 \cdot 10^{-3}$	0.2702
0.6	4π	0.1	0.5	$4.21 \cdot 10^{-4}$	$1.58 \cdot 10^{-3}$	0.2667
0.2	2π	0.4	0.1	$3.86 \cdot 10^{-4}$	$1.76 \cdot 10^{-3}$	0.2190
0.6	2π	0.1	0.4	$4.72 \cdot 10^{-4}$	$1.77 \cdot 10^{-3}$	0.2667
0.5	4π	0.7	0.1	$1.83 \cdot 10^{-4}$	$6.81 \cdot 10^{-3}$	0.2680

where the integral kernel r_ε is defined as

$$r_\varepsilon(x, x') \equiv \omega_\varepsilon(x - x') + \omega_\varepsilon(x + x') \tag{36}$$

The construction of single bump solution of (4) proceeds in the following way. First, we introduce $f_0^\varepsilon-$, $f_\tau^\varepsilon-$, and $f^\varepsilon-$ field models with output firing rate functions f_0, f_τ, defined in (17), and f, defined in (13), respectively.

We denote U_ε^0, U_ε^τ, and U_ε^* as the solutions of the $f_0^\varepsilon-$, $f_\tau^\varepsilon-$, and $f^\varepsilon-$ field models, respectively. U_ε^0 intersects θ at Δ_0^ε, i.e. $U_\varepsilon^0(\Delta_0^\varepsilon) = \theta$, and U_ε^τ intersects $\theta + \tau$ at Δ_τ^ε, i.e. $U_\varepsilon^\tau(\Delta_\tau^\varepsilon) = \theta + \tau$.

Due to the dependency of the parameter ε we also assume that the solution U_ε^τ may intersect $\theta + \tau$ more than one time. Let us define the values δ'

and δ'' such that

$$U_\varepsilon^\tau(x) > \theta + \tau, \quad \text{if } |x| < \Delta_\tau^\varepsilon - \delta',$$

$$U_\varepsilon^\tau(x) < \theta + \tau, \quad \text{if } |x| > \Delta_\tau^\varepsilon + \delta',$$

$$U_\varepsilon^0(x) > \theta, \qquad \text{if } |x| < \Delta_0^\varepsilon - \delta'',$$

$$U_\varepsilon^0(x) < \theta, \qquad \text{if } |x| > \Delta_0^\varepsilon + \delta''$$

A single bump solution of the $f_\tau^\varepsilon-$ field model can now be expressed as

$$U_\varepsilon^\tau(x) = \int_0^{\Delta_\tau^\varepsilon - \delta'} r_\varepsilon(x, x')dx' \tag{37}$$

Let us consider the equation (4). We check numerically if $\Delta_\tau^\varepsilon + \delta' < \Delta_0^\varepsilon - \delta''$ and split the interval $[0, \infty)$ into the following three subintervals $[0, \Delta_\tau^\varepsilon - \delta']$, $[\Delta_\tau^\varepsilon - \delta', \Delta_\tau^\varepsilon + \delta']$, $[\Delta_\tau^\varepsilon + \delta', \Delta_0^\varepsilon - \delta'']$, $[\Delta_0^\varepsilon - \delta'', \Delta_0^\varepsilon + \delta'']$, and $[\Delta_0^\varepsilon + \delta'', \infty)$. The bump solution U_ε can now be expressed as

$$\begin{aligned} U_\varepsilon(x) &= \int_0^{\Delta_\tau^\varepsilon - \delta'} r_\varepsilon(x, x')f(U_\varepsilon(x'))dx' + \int_{\Delta_\tau^\varepsilon - \delta'}^{\Delta_\tau^\varepsilon + \delta'} r_\varepsilon(x, x')f(U_\varepsilon(x'))dx' + \\ &+ \int_{\Delta_\tau^\varepsilon + \delta'}^{\Delta_0^\varepsilon - \delta''} r_\varepsilon(x, x')f(U_\varepsilon(x'))dx' + \int_{\Delta_0^\varepsilon - \delta''}^{\Delta_0^\varepsilon + \delta''} r_\varepsilon(x, x')f(U_\varepsilon(x'))dx' + \\ &+ \int_{\Delta_0^\varepsilon + \delta''}^{\infty} r_\varepsilon(x, x')f(U_\varepsilon(x'))dx' \end{aligned}$$

Since $U_\varepsilon(x') > \theta + \tau$ for $x' \in [0, \Delta_\tau^\varepsilon - \delta']$, then due to the properties of the firing rate function (13) $f(U_\varepsilon(x')) = 1$ on the interval $[0, \Delta_\tau^\varepsilon - \delta']$. Since $U_\varepsilon(x') < \theta$ for $x' \in [\Delta_0^\varepsilon + \delta'', \infty]$, then $f(U_\varepsilon(x')) = 0$ on the interval $[\Delta_0^\varepsilon + \delta'', \infty]$. Therefore, we obtain

$$\begin{aligned} U_\varepsilon(x) &= \int_0^{\Delta_\tau^\varepsilon - \delta'} r_\varepsilon(x, x')dx' + \int_{\Delta_\tau^\varepsilon - \delta'}^{\Delta_\tau^\varepsilon + \delta'} r_\varepsilon(x, x')f(U_\varepsilon(x'))dx' + \\ &\int_{\Delta_\tau^\varepsilon + \delta'}^{\Delta_0^\varepsilon - \delta''} r_\varepsilon(x, x')f(U_\varepsilon(x'))dx' + \int_{\Delta_0^\varepsilon - \delta''}^{\Delta_0^\varepsilon + \delta''} r_\varepsilon(x, x')f(U_\varepsilon(x'))dx' \end{aligned} \tag{38}$$

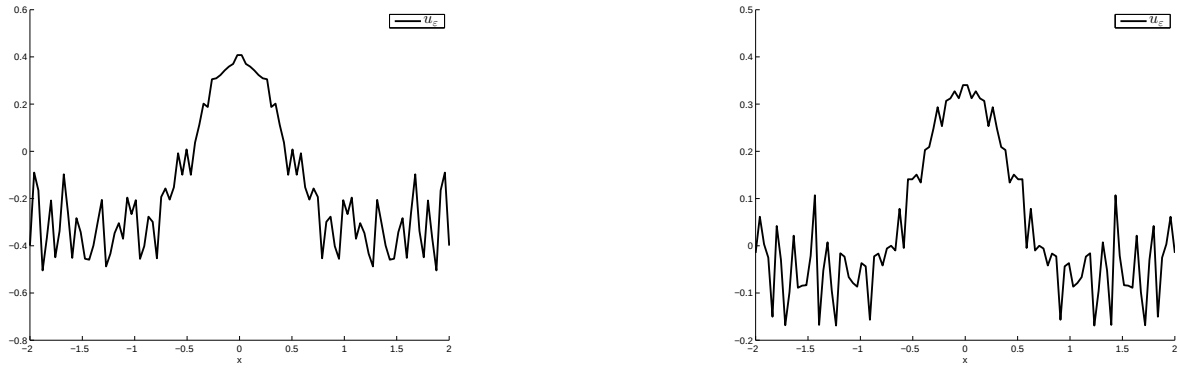

(a) (b)

Figure 5: The solutions U_ε^* of (4) in the case of the scaling function (10) (Fig. 6a) and the scaling function (11) (Fig. 6b). Input data: $\varepsilon = 10^{-5}$, $\gamma = 0.5$, $\theta = 0.1$, $\tau = 0.05$, $p = 2$, $\alpha = 2$, $K = 1.5$, $k = 2$, $M = 1$, $m = 1$.

and by taking into account (37) we get

$$\begin{aligned} U_\varepsilon(x) \quad &= U_\varepsilon^\tau(x) + \int\limits_{\Delta_\tau^\varepsilon - \delta'}^{\Delta_\tau^\varepsilon + \delta'} r_\varepsilon(x,x') f(U_\varepsilon(x'))dx' + \\ &\int\limits_{\Delta_\tau^\varepsilon + \delta'}^{\Delta_0^\varepsilon - \delta''} r_\varepsilon(x,x') f(U_\varepsilon(x'))dx' + \int\limits_{\Delta_0^\varepsilon - \delta''}^{\Delta_0^\varepsilon + \delta''} r_\varepsilon(x,x') f(U_\varepsilon(x'))dx' \end{aligned} \tag{39}$$

In the whole procedure we check numerically the positiveness of the kernel $r_\varepsilon(x,x')$ for all intervals of integration and finally by iterating (39) with the starting point (37) we find the solution $U_\varepsilon^*(x)$.

The next step in the iteration procedure consists of extending the solutions U_ε^* to functions defined on the product space $\mathbb{R} \times [0,1]$. Figs. 6a and 6b display graphically the solutions U_ε^* for the scaling functions (10) and (11), respectively, for $\varepsilon = 10^{-5}$.

We will now describe a method for constructing solutions $U(x,y)$ of (4) by

means of $U_\varepsilon^*(x)$. This procedure is based on the two-scale convergence introduced by Nguetseng [21] and the technique suggested by Visintin [26].

Let $Y = [0, 1)$. We say that a sequence $\{u_\varepsilon\} \in L^2(\mathbb{R})$ two-scale converges to $u \in L^2(\mathbb{R} \times Y)$ if

$$\lim_{\varepsilon \to 0} \{ \int_{\mathbb{R}} u_\varepsilon(x) \varphi(x, \frac{x}{\varepsilon}) dx \} = \iint_{\mathbb{R} \times Y} u(x, y) \psi(x, y) dx dy$$

for any smooth function $\psi : \mathbb{R} \times \mathbb{R} \to \mathbb{R}$ that is 1-periodic with respect to the second argument. In this case, we will conventionally write $u_\varepsilon \underset{2}{\to} u$. This convergence is crucial for obtaining the homogenized system (3) (see [23, 24, 25]). However, any numerical analysis of this convergence is a non-trivial task, and to the best of our knowledge this problem has not yet been explored. Below we suggest a numerical algorithm which is based on a more conventional convergence.

We proceed as follows: For any $\varepsilon > 0$, introduce the number $\mathcal{N}$ and the function $S_\varepsilon : \mathbb{R} \times Y \to \mathbb{R}$ defined as

$$\begin{gathered} \mathcal{N}(x) := \max\{n \in \mathbb{Z} : n \leqslant x\}, \quad x \in \mathbb{R} \\ S_\varepsilon(x, y) := \varepsilon(x/\varepsilon) + \varepsilon y, \quad \forall (x, y) \in \mathbb{R} \times Y, \quad \forall \varepsilon > 0 \end{gathered}$$

According to [26] we have the following equivalence

$$U_\varepsilon \underset{2}{\to} U \text{ in } L^p(\mathbb{R} \times Y) \;\; \Leftrightarrow \;\; U_\varepsilon \circ S_\varepsilon \to U \text{ weakly in } L^p(\mathbb{R} \times Y) \tag{40}$$

to find the 1-periodic extension $U(x, y)$ of the function $U_\varepsilon^*(x)$. Here $U_\varepsilon \circ S_\varepsilon(x, y) = U_\varepsilon(S_\varepsilon(x, y))$.

By using the iteration scheme developed in [11] we obtain numerically the vector $U_\varepsilon(x)$. The difficulty of the numerical simulations consists of finding the superposition $U_\varepsilon^*(x) \circ S_\varepsilon(x, y)$ since $U_\varepsilon^*(x)$ is found as a vector. Here we outline the numerical method for solving this problem.

We proceed as follows:

- Find explicitly the matrix $S_\varepsilon(x, y)$ for $x \in [-x_{st}, x_{st}]$, $y \in [0, 1]$ with step h.

- Find the extended matrix $S_\varepsilon^{ext}(x,y)$ for $[-x_{st}-x_0, x_{st}+x_0]$, $y \in [0,1)$ with smaller step h/k, $k \in \mathbb{N}$, $k > 1$.
- Find the matrix $Index$ which consists of the indexes of the elements of the matrix S_ε in the matrix S_ε^{ext}.
- Find a matrix U_ε^{ext} by using the iteration formula (39) which consists of the columns $U_{\varepsilon j}^{ext}$ for $x = S_{\varepsilon j}^{ext}$, where $S_{\varepsilon j}^{ext}$ is column j in the matrix S_ε^{ext}.
- Select the elements from the matrix U_ε^{ext} only with the indexes from $Index$ matrix.
- Get the matrix U which is numerical superposition of the $U_\varepsilon^*(x)$ and $S_\varepsilon(x,y)$.

To show that our method works, we apply it to the example of the superposition of connectivity kernel ω_ε in the case of the scaling function (10) and $S_\varepsilon(x,y)$ which we can find either explicitly by plotting the composition $\omega_\varepsilon(S_\varepsilon(x,y))$ or implicitly by using the superposition method. The results are shown in the Fig. 6 for $\varepsilon = 10^{-4}$. The next step in the construction procedure consists of finding the numerical superposition $U_\varepsilon(x)$ and $S_\varepsilon(x,y)$ for the connectivity kernels (10) and (11).

The Figs. 7a and 7b in the case of wizard hat scaling function (10) and the difference of Gaussian scaling functions (11), respectively, show that the solutions $U(x,y)$ do not change with the local variable y. This supports numerically the hypothesis that the bump solutions are y-independent.

4. Iteration scheme for bump solutions of the homogenized Amari equation

The previous sections give numerical evidence for nonexistence of y-dependent stationary solutions. This indicates that the homogenized Amari model (3) plays a key role in the study of bump solutions. Motivated by this, we embark in this section on formulating an iteration scheme for construction of single bump solutions of this model. The numerical procedure is based on a modification of the scheme developed in Oleynik *et al.* [11].

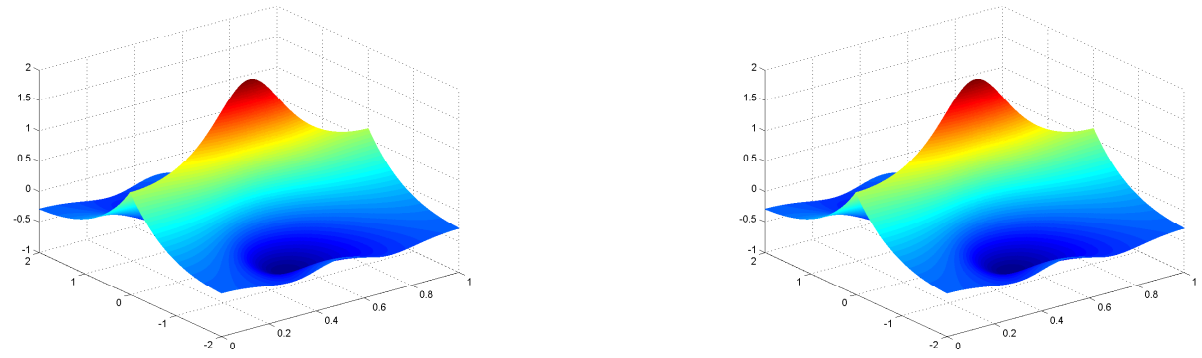

(a) (b)

Figure 6: The superposition $\omega_\varepsilon(x) \circ S_\varepsilon(x, y)$ implicitly (a) and explicitly (b) in the case of the scaling function (10). Input data: $\alpha = 2$, $\gamma = 0.5$, $\varepsilon = 10^{-4}$.

We first observe that the mean value of the connectivity kernel $\langle\omega\rangle$ satisfies the same properties as the connectivity kernel ω due to the properties of the scaling function φ and footprint function σ. Fig. 8 shows the mean value of the connectivity function $\langle\omega\rangle$ for different parameters γ: $\gamma = 0$, $\gamma = 0.3$, $\gamma = 0.5$, $\gamma = 0.7$ in the cases of the scaling functions (10)– (a) and the scaling function (11) – (b).

We then investigate the existence/nonexistence of the single bump solutions U^0 and U^τ of the f_0- and $f_\tau-$ model, respectively. We proceed by using the pinning function technique developed in Svanstedt *et al.* [24]. The graph of the pinning function (23) for different values of heterogeneity parameter γ is depicted in the cases of the scaling function (10) (Fig. 9a) and the scaling function (11) (Fig. 9b). We observe that the interval of existence of single bumps is decreasing when we increase the heterogeneity. Numerically, we observe that for fixed values of θ and γ there is a τ-interval, say $[0, \tau_{cr}]$, for which we have two single bump solutions. Fig. 9 shows a plot of τ_{cr} for some selected values of heterogeneity parameter. For $\tau > \tau_{cr}$ there are no bumps.

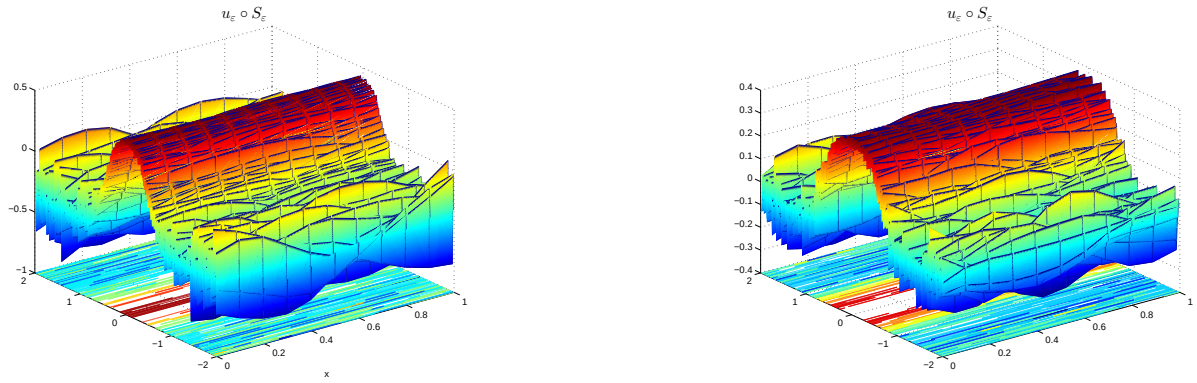

(a) (b)

Figure 7: The superposition of the $U_\varepsilon^*(x) \circ S_\varepsilon(x, y)$ in the case of the scaling function (10) - (a) and the scaling function (11) - (b). Input data: $\varepsilon = 10^{-5}$, $\gamma = 0.5$, $\theta = 0.1$, $\tau = 0.05$, $p = 2$, $\alpha = 2$, $K = 1.5$, $k = 2$, $M = 1$, $m = 1$.

We have plotted the number of single bump solutions as a function of the smoothness parameter τ and the heterogeneity parameter γ in the cases of the scaling function (10) (Fig. 10a) and the scaling function (11) (Fig. 10b). This plot reveals that the τ-interval for existence of single bump solutions decreases with the degree of heterogeneity.

We now assume that the smoothness parameter τ and the heterogeneity parameter γ are designed in such a way so that single bump solutions U_0 and U_τ of the f_0- and $f_\tau-$ field model exist, i.e. that (τ, γ) belongs to dark green regions in Fig. 10. By assumption this means that U_0 and U_τ have unique positive intersection points with the threshold values θ and $\theta + \tau$ in Δ_0 and Δ_τ, respectively, i.e. $U_0(\Delta_0) = \theta$, $U_\tau(\Delta_\tau) = \theta + \tau$. We now observe that if the equation (6) has a spatially symmetric stationary solution U^*, it satisfies the fixed point problem

$$U^* = T_f U^* \tag{41}$$

where

$$(T_f U)(x) = U_\tau(x) + \int_{\Delta_\tau}^{\Delta_0} r(x, x') f(U(x'))dx', \tag{42}$$

with the integral kernel r defined as

$$r(x, x') \equiv \langle\omega\rangle(x - x') + \langle\omega\rangle(x + x') \tag{43}$$

In accordance with the squeezing result (20), we have the Kishimoto–Amari type of bound

$$U_\tau(x) \leq U^*(x) \leq U_0(x) \tag{44}$$

In order to construct the single bump solution U^* of $f-$ field model with this property, we first make use of the following result which we easily derive by making a slight modification of the fixed point theorem in Oleynik *et al.* [11] which we here present without proof:

Theorem 1. *Let the operator $T_f : [U_\tau, U_0] \subset \mathcal{B} \to \mathcal{B}$ be defined by (42), where $\mathcal{B}$ is chosen to be either $L_2([\Delta_\tau, \Delta_0])$ or $C([\Delta_\tau, \Delta_0])$. Assume that $r(x, x') \geq 0$ for $x, x' \in [\Delta_\tau, \Delta_0]$. Then the operator T_f has a fixed point in $[U_\tau, U_0]$. Moreover, the sequences $\{T_f^n U_\tau\}$ and $\{T_f^n U_0\}$ converge to the minimal and maximal fixed point of the operator T_f, respectively. If $\lim_{n\to\infty} T_f^n U_\tau = \lim_{n\to\infty} T_f^n U_0$, then the fixed point is unique and given by U^*.*

Notice that this theorem yields the single bump solution U^* restricted to the interval $[\Delta_\tau, \Delta_0]$. The next step in the iteration procedure consists of extending this solution to the whole x-axis. Following Oleynik *et al.* [11], we do this in the following way: Introduce the function

$$\Phi(x, x') = \int_0^{x'} \int_0^1 r(x, z)dz, \quad x, x' \in \mathbb{R}, \ x' > 0, \tag{45}$$

with

$$\frac{\partial \Phi}{\partial x}(x, x') = \int_0^1 \frac{1}{\sigma(y)} \Big(\varphi[\frac{x' - x}{\sigma(y)}] - \varphi[\frac{x' + x}{\sigma(y)}] \Big) dy.$$

The following theorem guarantees that we can do the desired extension to the whole real axis:

Theorem 2. *If*

1. *U_0 is a decreasing function on the interval $[\Delta_\tau, \Delta_0]$, i.e.*

$$\frac{\partial \Phi}{\partial x}(x, \Delta_0) < 0, \quad \forall x \in [\Delta_\tau, \Delta_0]$$

and U_τ is a decreasing function on the interval $[\Delta_\tau, \Delta_0]$, which is equivalent to

$$\frac{\partial \Phi}{\partial x}(x, \Delta_\tau) < 0, \quad \forall x \in [\Delta_\tau, \Delta_0],$$

2. $$\int_{\Delta_\tau}^{\Delta_0} \Big| \frac{\partial}{\partial x} \langle r \rangle (x, x') \Big| dx' < \frac{\partial \Phi}{\partial x}(x, \Delta_\tau), \ \forall x \in [\Delta_\tau, \Delta_0],$$

3. *the function Φ possesses the following properties*
   - $\Phi(x, z) \leqslant \theta \ \forall x > \Delta_0, \quad z \in [\Delta_\tau, \Delta_0]$
   - $\Phi(x, z) \leqslant \theta + \tau \ \forall x > \Delta_\tau, \quad z \in [\Delta_\tau, \Delta_0]$

then the fixed point U^* defined on the interval $[\Delta_\tau, \Delta_0]$ can be extended to a bump solution $U(x)$ of (6) defined on $\mathbb{R}$ such that $U(x) > \theta + \tau \ \forall x \in [0, \Delta_\tau]$ and $U(x) < \theta \ \forall x \in (\Delta_0, \infty)$.

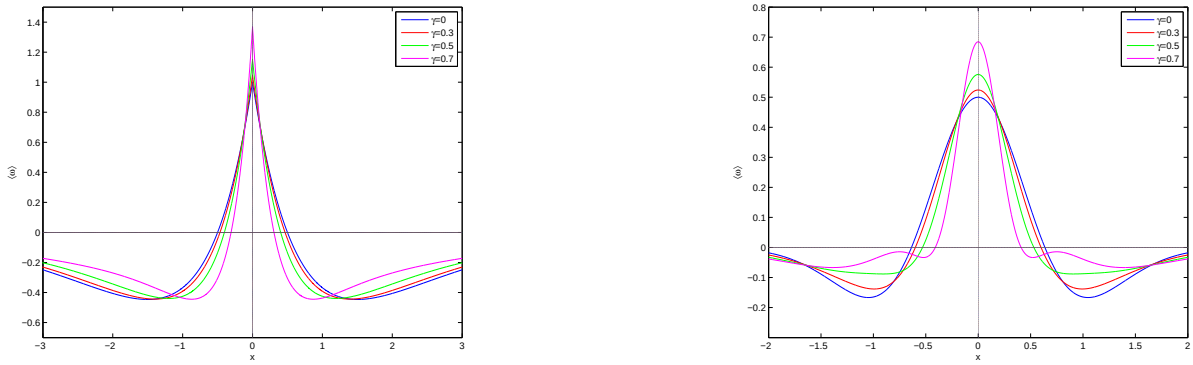

(a) (b)

Figure 8: The mean value of the connectivity kernel ω in the case of the scaling function (10) – (a) and the scaling function (11) – (b) for different values γ. Input data: $\alpha = 2$, $K = 1.5$, $k = 2$, $M = 1$, $m = 1$, $\gamma = 0$, $\gamma = 0.3$, $\gamma = 0.5$, $\gamma = 0.7$.

We omit the proof of this result.

If $\langle\omega\rangle(\Delta_0) < 0$, then $W(L, \gamma)$ is decreasing. Then there exists $\tau > 0$ such that $W(2\Delta_\tau) = \theta + \tau$ $(\Delta_\tau < \Delta_0)$, and therefore a $2\Delta_\tau-$ solution. Since there is a $2\Delta_0-$ solution of the f_0- field model, i.e. $\Phi(\Delta_0, \Delta_0) = \theta$ then there exists a value $\tau > 0$ such that $\Phi(\Delta_\tau, \Delta_\tau) = \theta + \tau$ for $\Delta_\tau < \Delta_0$.

Numerically we can check that the conditions of Theorem 1 and Theorem 2 are verified in the cases of the scaling function (10) and the scaling function (11).

In Figs. 11b and 12b we have plotted U^* on the interval $x \in [\Delta_\tau, \Delta_0]$ obtained by iteration from U_0 and U_τ when f is given as in (13) for different values of the heterogeneity parameter. We clearly observe that U^* is bounded in-between from below by U_τ and from above by U_0 on the interval $x \in [\Delta_\tau, \Delta_0]$. In Figs. 11a and 12a we extend these solutions to the whole x-axis.

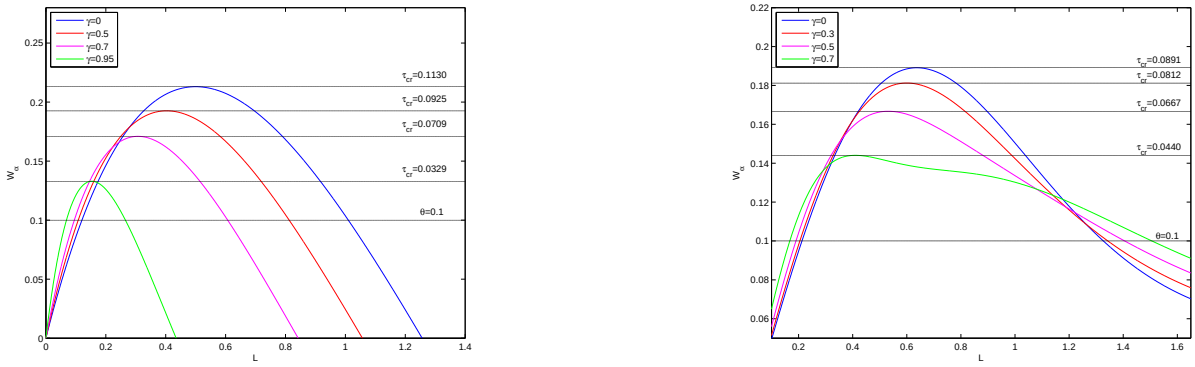

(a) (b)

Figure 9: The pinning function (23) for different values of the heterogeneity parameter γ with corresponding critical values of the smoothness parameter τ in the case of the scaling function (10) - (a) and the scaling function (11) - (b). Input data: $\alpha = 2$, $K = 1.5$, $k = 2$, $M = 1$, $m = 1$, $p = 2$, $\theta = 0.1$, $\gamma = 0$, $\tau_{cr} = 0.1130$, $\gamma = 0.5$, $\tau_{cr} = 0.0925$, $\gamma = 0.7$, $\tau_{cr} = 0.0709$, $\gamma = 0.95$, $\tau_{cr} = 0.0329$, $\gamma = 0$, $\tau_{cr} = 0.0891$, $\gamma = 0.3$, $\tau_{cr} = 0.0812$, $\gamma = 0.5$, $\tau_{cr} = 0.0667$, $\gamma = 0.7$, $\tau_{cr} = 0.0440$.

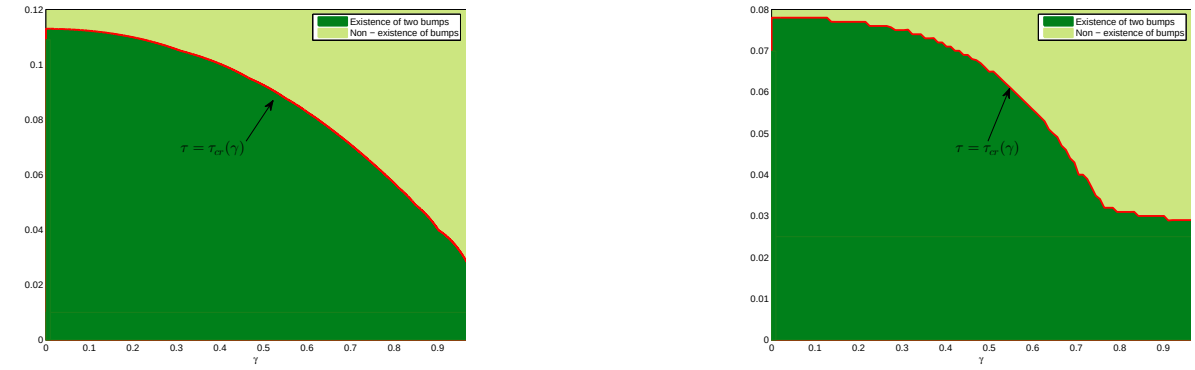

(a) (b)

Figure 10: The number of single bump solutions as a function of smoothness parameter τ and the heterogeneity parameter γ for a given threshold value θ: a) in the case of the scaling function (10) and b) the scaling function (11). Input data: $\theta = 0.1$, $\alpha = 2$, $K = 1.5$, $k = 2$, $M = 1$, $m = 1$.

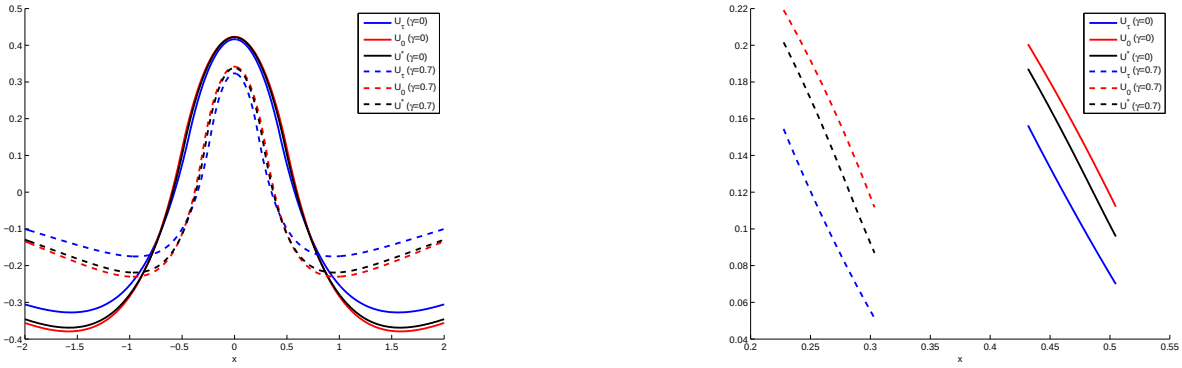

(a) (b)

Figure 11: The functions U_τ, U_0, U^* as solutions of the $f_\tau-$, f_0- and $f-$ field model, respectively, in the case of the scaling function (10). Input data: $\alpha = 2$, $p = 2$, $\theta = 0.1$, $\tau = 0.05$, $\gamma = 0$, $\gamma = 0.7$.

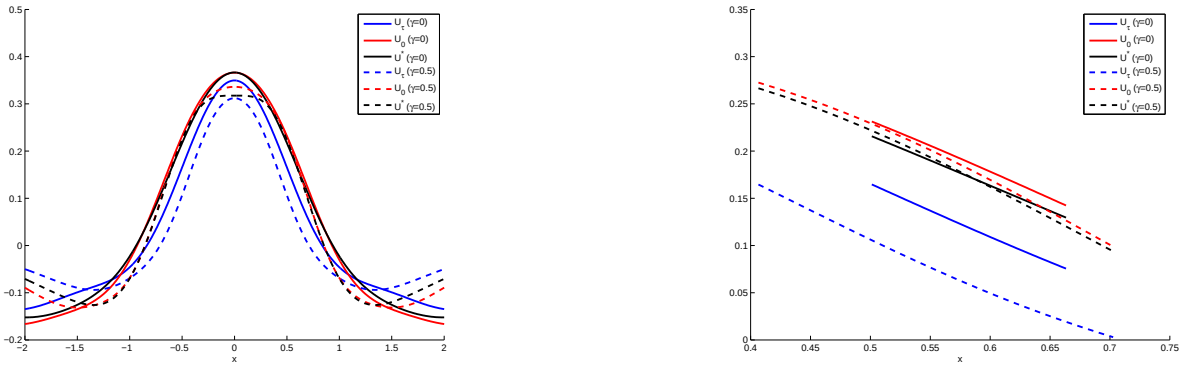

(a) (b)

Figure 12: The functions U_τ, U_0, U^* as solutions of the $f_\tau-$, f_0- and $f-$ field model, respectively, in the case of the scaling function (11). Input data: $K = 1.5$, $k = 2$, $M = 1$, $m = 1$, $p = 2$, $\theta = 0.1$, $\tau = 0.05$, $\gamma = 0$, $\gamma = 0.5$.

5. Conclusions and outlook

The present paper is devoted to numerical construction of single bump solutions of the homogenized Amari model for steep firing rate functions and their Heaviside limit.

First, we have demonstrated in detail two attempts to construct solutions of (5) which exhibit a variation in the local variable y. The first attempt was based on an extension of the pinning functions technique developed in Svanstedt *et al.* [24]. This method is applicable to the case when the firing rate function is given by means of the Heaviside step function (14). In the second attempt we made use of a combination of the iteration method for single bumps developed in Oleynik *et al.* [11] and the superposition method outlined in Visintin [26]. This method was designed for constructing the single bump solutions of the homogenized Amari equation (3) in the case of sigmoidal firing rate function (13). Numerical experiments based on these attempts clearly indicated that the single bump solutions do not exhibit a variation with the local variable y. This gave support to the idea that the homogenized model (3) should crucial play a role in the theory and should be the focus of the study.

As a consequence, we developed an iteration scheme for constructing single bump solutions of (6) in the case of sigmoidal firing rate function (13) based on Oleynik *et al.* [11]. The actual bumps U^* are bounded by two single bump solutions U^τ and U^0 in the f_0- and $f_\tau-$ field model of (6) by a Kishimoto–Amari type of bound (44). U^0 and U^τ are constructed by means of the pinning function technique from Svanstedt *et al.* [24]. We detected regions of existence/nonexistence of U^0 and U^τ as a function of the smoothness parameter τ and the heterogeneity parameter γ. The plot (10) reveals that the τ-interval for existence of single bump solutions decreases with the degree of heterogeneity. The construction of U^* was then carried out by means of fixed point iteration scheme based on Oleynik *et al.* [11].

In our future work we aim at rigorous studying the existence of single bump solutions of (5) from a mathematical perspective. We conjecture that this problem can be tackled by using techniques from nonlinear functional analysis and the degree theory. In line with that we will investigate the possibility of developing an iteration scheme for the fixed point problem (5) for more

general firing rate functions.

6. Acknowledgements

The authors would like to thank Professor Bjørn Nielsen (Norwegian University of Life Sciences), Dr. Jean Louis Woukeng (University of Dschang, Cameroon), Dr. Anna Oleynik (Centre of Interdisciplinary Mathematics, Uppsala University, Sweden), Professor LieJune Shiau (University of Houston, Clear Lake, USA) and Professor Anders Holmbom (Mid Sweden University, Sweden) for many fruitful and stimulating discussions during the preparation of this paper. The authors will also like to thank M.Sc Sergio Haram Sarmiento (Centre for Integrative Genetics, Norwegian University of Life Sciences) for computer assistance.

[1] S. Amari, *Dynamics of pattern formation in lateral-inhibition type neural fields*, Biological Cybernetics. **27**, (1977), pp. 77–78.

[2] S. Coombes, *Waves, bumps, and patterns in neural field theories*, Biological Cybernetics **93** (2005) 91–108.

[3] P. Bressloff, *Spatiotemporal dynamics of continuum neural fields*, J. Phys. A: Math. Theor. 45,(2012), 033001

[4] C. R. Laing and W. C. Troy, *PDE methods for non-local models*, SIAM J Appl Dyn Syst. Vol 2, no. 3, (2003), pp. 487–516.

[5] A. J. Elvin, C. R. Laing, R. I. McLachlan and M. G. Roberts, *Exploiting the Hamiltonian structure of a neural field model*, Physica D, Vol. 239, (2010), pp. 537–546.

[6] K. Kishimoto and S. Amari, *Existence and stability of local excitations in homogeneous neural fields*, J. Math. Biology, **7** (1979), pp. 303–318.

[7] O. Faugeras, R. Veltz and G. Grimbert, *Persistent neural states: stationary localized activity patterns in nonlinear continuous n - population, q - dimensional neural networks*, Neural Computation, **21**: 1, (2009) pp. 147–187.

[8] R. Veltz and O. Faugeras, *Local/Global Analysis of the Stationary Solutions of Some Neural Field Equations*, SIAM J. APPLIED DYNAMICAL SYSTEMS Vol. 9, No. 3, (2010) pp. 954-998.

[9] A. Oleynik, A. Ponosov and J. Wyller, *On the properties of nonlinear nonlocal operators arising in neural field models*, J. Math. Anal. Appl. **398** (2013) pp. 335 - 351.

[10] S. Coombes and H. Schmidt, *Neural fields with sigmoidal firing rates: approximate solutions*, Discrete and Continuous Dynamical Systems Series A, Vol 28, (2010), pp. 1369 – 1379.

[11] A. Oleynik, A. Ponosov, and J. Wyller, *Iterative schemes for bump solutions in a neural field model*. Differential Equations and Dynamical Systems, Springer India, 2013.

[12] J. Xin, *An Introduction to Fronts in Random Media*, SIAM Review, 42, (2000), p. 161.

[13] J. Xin, *An Introduction to Fronts in Random Media*, Surveys and Tutorials in the Applied Mathematical Sciences, Springer Verlag, (2009).

[14] P. C. Bressloff, *Traveling fronts and wave propagation failure in an inhomogeneous neural network*, Physica D 155 (2001), pp. 83–100.

[15] P. C. Bressloff, *Spatially periodic modulation of cortical patterns by long-range horizontal connections*, Physica D 185, (2003), pp. 131–157.

[16] P. C. Bressloff, S. E. Folias, A. Pratt and Y-X Li, *Oscillatory waves in inhomogeneous neural media*, Phys. Rev. Lett. 91:178101 (2003);

[17] X. Huang, W.C. Troy, Q. Yang, H. Ma, C.R. Laing, S.J. Schiff, J.-Y. Wu, *Spiral waves in disinhibited mammalian neocortex* J. Neurosci. 24 (44) (2004), pp. 9897–9902.

[18] Z. P. Kilpatrick, S. E. Folias and P. C. Bressloff, *Traveling pulses and wave propagation failure in an inhomogeneous neural network*, SIAM J. Appl. Dyn. Syst. 7, (2008), pp. 161–185.

[19] S. Coombes and C. R. Laing, *Pulsating fronts in periodically modulated neural field models*, Phys. Rev. E. 83 (2010) 011912.

[20] L.- E. Persson. L. Persson, N. Svanstedt and J. Wyller, *The Homogenization Method. An introduction*. Studentlitteratur. 1993.

[21] G. Nguetseng, *A general convergence result of a functional related to the theory of homogenization*, SIAM J. Math. Anal. 20 (1989), pp. 608–623.

[22] D. Lukkassen, G. Nguetseng and P. Wall, *Two-scale convergence*,Int. J. Pure Appl. Math. 2 (2002), pp. 35–86.

[23] N. Svanstedt and J. L. Woukeng, *Homogenization of a Wilson - Cowan model for neural fields in a bounded domain*. Nonlinear Analysis: Real World Applications, 14, (2013), pp. 1705–1715.

[24] N. Svanstedt, J. Wyller, E. Malyutina, *A one population Amari - model with periodic microstructure*, Nonlinearity 27 (2014), pp. 1391–1417.

[25] S. Coombes, C. Laing, H. Schmidt, N. Svanstedt and J. Wyller, *Waves in random neural media*, Discrete and Continuous Dynamical Systems — Series A, 32 (2011) pp. 2951–2970.

[26] A. Visintin, *Two-scale convergence of some integral functionals*, Calc. Var. Partial Differential Equations 29, (2007), pp. 239–265.

[27] J. J. Mor, D. C. Sorensen, *Computing a Trust Region Step*, SIAM Journal on Scientific and Statistical Computing, Vol. 3 (1983) pp. 553 - 572.